Biosensors and Bioelectronics 101 (2018) 174–180

Contents lists available at ScienceDirect

Biosensors and Bioelectronics

journal homepage: www.elsevier.com/locate/bios

An aptasensor based on heparin-mimicking hyperbranched polyester with anti-biofouling interface for sensitive thrombin detection

Yanlian Niu, Meilin Chu, Ping Xu, Shuangshuang Meng, Qian Zhou, Wenbo Zhao*, Bo Zhao, Jian Shen*

National and Local Joint Engineering Research Center of Biomedical Functional Materials, School of Chemistry and Materials Science, Nanjing Normal University, Nanjing 210023, China

ARTICLE INFO

Keywords:
Heparin-mimicking
Hyperbranched polyester
Whole blood
Aptasensor
Thrombin

ABSTRACT

In this paper, novel heparin-mimicking hyperbranched polyester nanoparticles (HBPE-SO_3 NPs) with abundant of sulfonated acid functional groups were synthesized, and their antithrombogenicities were further evaluated. Further, a label-free electrochemical aptamer biosensor (aptasensor) based on HBPE-SO_3 NPs modified electrode was developed for thrombin (TB) detection in whole blood. Meanwhile, the anti-biofouling properties of different modified electrodes were studied by whole blood and platelet adhesion test, hemolysis assay and morphological changes of red blood cells *in vitro*. Besides, the thrombin-binding aptamer was selected as receptor for the proposed aptasensor, which has excellent binding affinity and selectivity for TB. When binding to TB, the electron transfer taking place at the modified electrode interface was inhibited that can attribute to the stereohindrance effect, resulting in the decreased current response. This aptasensor showed excellent electrochemical properties with a wide detection range and a low detection limit of 0.031 pM (S/N = 3), and provided high selectivity, long-term stability and good reproducibility. Finally, the sensitively detection of TB in whole blood samples directly was achieved by this aptasensor we proposed, which suggested its great potential for TB detection in the clinic.

1. Introduction

Hyperbranched polymers (HBPs) have three-dimensional topological structures and series of particular properties including high density of functional groups, intramolecular cavities, nano-sized effect and so on, which can be attributed to the highly branched globular and dendritic molecular architectures (Ding et al., 2012). In consequence, HBPs exhibit wide applications in a variety of areas, for instance, nanotechnology, biomedical, additives and composite materials (Wu et al., 2015). Our group reported novel new hyperbranched zwitterionic structures-modified bare metal stents with good biocompatibility, which had enormous potential in inhibit thrombosis, minimize restenosis of coronary artery diseases and other biological applications (Wang et al., 2013a, 2013b, 2014). Furthermore, the great development in synthetic strategies and easy to modify give rise to diverse HBPs with desirable functional properties (Zheng et al., 2015; Yu et al., 2010). Brooks had synthesized and characterized series of hyperbranched polyglycerols that functionalized with different ligands, and obtained the functional polymer with promoting hemostasis properties *via* precisely controlled the proportions of different ligands (Wen et al., 2016).

Based on the crucial roles of thrombin (TB) in coagulation cascade, hemostasis and thrombosis, of which the detection and quantification of TB in biological serum or other complex samples are great of significance for clinical diagnosis applications (Shen et al., 2017; Xu et al., 2015). Electrochemical bioanalytical method, with lots of merits such as simple preparation and operation, high sensitivity, great selectivity and anti-interference performance, wide detection range and so forth (Cui et al., 2016), was widely applied in concentration detection of TB. Up to now, however, the most of reported electrochemical methods of TB concentration detection were mainly performed in serum samples (Shen et al., 2017; Xu et al., 2015; Xiao et al., 2005; Sun et al., 2014; Gao et al., 2015). Generally, the serum samples were obtained by factitious operations, especially additional centrifugal treatment, accordingly, both factitious and long treating time will introduce inevitable errors for the TB detection. Thus, it's great significance of designing and preparing an electrochemical biosensor that can be used in whole blood directly.

When the conventional electrodes as foreign materials contact with blood, the coagulation cascade reaction will occur correspondingly. This will lead to the biological pollution of blood components that

* Corresponding authors.
E-mail addresses: zhaowenbo@njnu.edu.cn (W. Zhao), jshen@njnu.edu.cn (J. Shen).

http://dx.doi.org/10.1016/j.bios.2017.10.037
Received 20 August 2017; Received in revised form 14 October 2017; Accepted 16 October 2017
Available online 18 October 2017

coating on the electrode surface (Huang et al., 2016). Therefore, the anticoagulant or anti-biofouling property of the electrode substrates is the key problem to solve for biosensor that used in the whole blood directly (Huang et al., 2014).

Heparin has always been regarded as an injectable anticoagulant in clinical (He et al., 2017; Paluck et al., 2016). Some research groups have demonstrated that the excellent anticoagulant property of heparin can be attributed to the abundant of functional groups (OSO_3^-, $NHSO_3^-$ and COO- groups) in the molecular architecture (Wang et al., 2015; Tamada et al., 2002), which gave heparin a total negative net charge (Capila and Linhardt, 2002). Herein, based on the abundant terminal groups and the nano-sized effects of HBPs, a novel of heparin-mimicking hyperbranched polyester nanoparticles (HBPE-SO_3 NPs) with controlled structure, sulfation and purity were synthesized, and their blood compatibilities were evaluated *in vitro*. Additionally, a label-free aptamer biosensor (aptasensor) based on HBPE-SO_3 NPs modified electrode was designed and developed for sensitive detection of TB *via* the layer-by-layer self-assembly methods. And the fabricated process of aptasensor, the electrochemical performance and the real samples measurements in whole blood were presented in detail.

2. Experimental section

2.1. Synthesis of HBPE-SO_3 NPs

Second-generation aliphatic hyperbranched polyester (HBPE-OH) was prepared using quasi-one-step method with abundant of terminal hydroxyl groups and then modified by sulfonic acid groups to get HBPE-SO_3 NPs, which were presented in a previous paper by our group (Han et al., 2013). Briefly, in the presence of *p*-toluenesulfonic acid as catalyst, the esterification reaction between trimethylol propane and 2,2-bis (hydroxymethyl)propionic acid was carried out at 140 °C to form HBPE-OH. And the final product was obtained by precipitating crude polymer from acetone in n-hexane. Second, to a 150 mL three-necked flask with a magnetic stir bar, the mixtures of HBPE-OH and excess NaH in anhydrous tetrahydrofuran were added to react under reflux overnight before adding 1,3-propane sultone, and then allowed to react for another 12 h under reflux. The resulting solution was filtered, then, the crude product was exhaustively dialyzed by pure water, and the purified product of HBPE-SO_3 was obtained. In addition, the antithrombogenicity of HBPE-SO_3 NPs was further evaluated by coagulative time tests, including activated partial thromboplastin time (APTT), prothrombin time (PT) and thrombin time (TT). The detailed experimental procedures were described in Supporting information.

2.2. Characterization of TBA/HBPE-SO_3

When binding to TB, thrombin-binding aptamer (TBA), a 15-mer G-rich DNA oligonucleotide (5′-GGT TGG TGT GGT TGG-3′) (Xi et al., 2015), could change its secondary structure from random coil to chair-like antiparallel G-quadruplex (Heydari-Bafrooei et al., 2016; Aaldering et al., 2017). Thus, the ultraviolet visible (UV–vis) spectrophotometer was employed to measure the configuration transition of TBA when incubating with HBPE-SO_3 NPs for further investigating the biocompatibility of HBPE-SO_3.

2.3. Construction of TBA/HBPE-SO_3/Au/MPTMS/GCE and measurements

Prior to modification, the glassy carbon electrode (GCE) was typically polished by alumina slurry in succession, and then sonicated in pure ethanol and distilled water, finally allowed to air-dry at room temperature for further to use (Arab Chamjangali et al., 2015). The construction process of proposed aptasensor was presented in Scheme 1 with layer-by-layer self-assembly method. Firstly, 8.0 μL of 0.1% 3-mercaptopropyltrimethoxysilane (MPTMS) solution (anhydrous alcohol as solvent) was successfully grafted onto the pretreated electrochemical electrode surface for increasing the amount of hydroxyl groups on the electrode surface (Hao et al., 2007), and dried in air. The obtained MPTMS/GCE was modified by 8.0 μL of positively charged Au NPs (see Supporting information) aqueous with the terminal thiol groups of MPTMS molecule, subsequently. Then, 8.0 μL of HBPE-SO_3 NPs (0.1 mg/mL) was immobilized by electrostatic absorption, and the obtained HBPE-SO_3/Au/MPTMS/GCE was stored at 4 °C before use.

Finally, the HBPE-SO_3 modified GCE was immersed into 1.0 mL of a mixing solution containing 1.0 μM TBA (5′-amino-modified), 0.1 M NaCl and 4 mM EDTA for 24 h, which was adjusted pH to 7.4 with 20 mM Na_2HPO_4, followed by rinsing with phosphate buffered saline (PBS, 0.1 M, pH 7.4) to remove unreacted TBA. Here, TBA was grafted onto the surface of modified GCE *via* weak electrostatic interactions. The TBA/HBPE-SO_3/Au/MPTMS/GCE was then incubated with 2% bovine serum albumin (BSA) to block possible active sites against nonspecific adsorption. The other different modified electrodes that used as contrast groups were prepared by the same modified method. Since the target molecule of TB was appeared, a complex of G-quadruplex-TB was formed and such a complex increased the steric hindrance that greatly restrained the electrons transfer occurring on the electrode surface. When not in use, the electrodes were stored at 4 °C.

2.4. Hemocompatibility tests of HBPE-SO_3 NPs modified electrodes

2.4.1. Whole blood and platelet adhesion test

In detail, for evaluation of the anti-biofouling effect of HBPE-SO_3 NPs modified the electrode surface, the whole blood and platelet adhesion tests were performed. However, the GCE was very difficult to be tailored into pieces for test. So, here, the indium tin oxide (ITO) electrodes with the same modified method instead of GCE were placed in the 24-well microplates and immersed in PBS for 24 h. After removing the PBS, the fresh rabbit whole blood with sodium citrate were dropped on each well with an incubation time of 1 h at 37 °C, followed by removing the blood with an aspirator and rinsing three times with 1 mL PBS. Then, 1 mL of 2.5 vol% glutaraldehyde in PBS was used to immobilize the bounded blood cells for 30 min at room temperature. The electrodes were washed with PBS again and then subsequently dehydrated by a series of ethanol-water mixing solutions (50%, 60%, 70%, 80%, 90%, 95% and 100% (v/v)) for 30 min each and allowed to air-dry. The electrodes were coated with gold, and then the treated ITO surface was observed by scanning electron microscopy (SEM). Instead of whole blood, platelet rich plasma, which was prepared by centrifuging anticoagulated whole blood at 800 rpm for 15 min, was applied to clarify the adhesion of platelet using the same procedures as described above (Wang et al., 2013a, 2013b).

And other hemocompatible experimental procedures including hemolysis assay and morphological changes of red blood cells (RBCs) were also presented in Supporting information.

3. Result and discussion

3.1. Characterization of the HBPE-SO_3 NPs and Au NPs

Learned from the previous literature, the HBPE-SO_3 NPs were incomplete sulfonated-terminal modified with retaining part of hydroxyl groups, and well-distributed in aqueous with nanoscale fake-spherical morphology (Han et al., 2013). Furthermore, the organic compound, 4-dimethylaminopyridine was adopted to realize the phase transfer of Au NPs from organic to aqueous solutions. And the Au NPs with positively charged was obtained ($+14.5 \pm 2.3$ mV, Fig. S2). As shown in Fig. S3, the Au NPs had an ultraviolet absorption peak at 528 nm, and their hydration radius were 60.3 ± 0.5 nm by dynamic light scattering (DLS), which was consistent with the results observed by transmission electron microscopy (TEM).

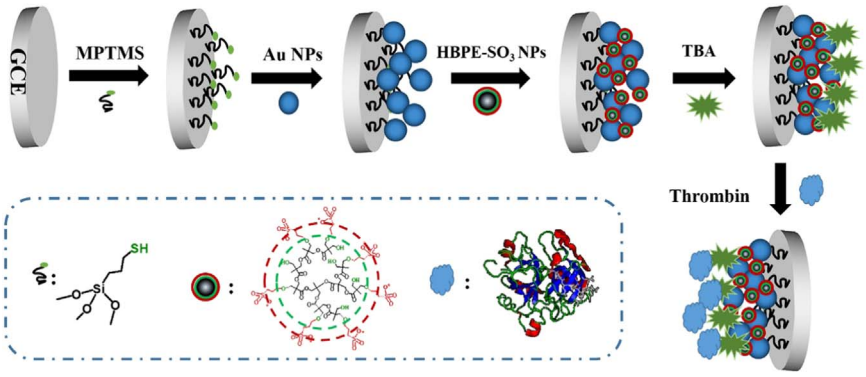

Scheme 1. Schematic illustration of the fabrication process of the TB aptasensor *via* layer-by-layer self-assembly modification method.

3.2. Biocompatibility of the HBPE-SO_3 NPs and modified electrodes

3.2.1. Anticoagulation properties of HBPE-SO_3 NPs

APTT, PT and TT were considered to a crucial for anticoagulant properties assay (Cuker et al., 2014; Zhang et al., 2008). Therefore, in order to evaluate the antithrombogenicity of HBPE-SO_3 NPs, APTT, PT and TT were studied to monitor the coagulation time of HBPE-SO_3 NPs *in vitro*, which was compared with that of heparin as shown in Fig. 1. Results showed that in the concentration range of 0.05, 0.25, 0.5 mg/mL, the APTT (Fig. 1A), PT (Fig. 1B) and TT (Fig. 1C) values of the HBPE-SO_3 NPs were higher than that of HBPE-OH, indicating that HBPE-SO_3 had good anticoagulant performance, and interestingly, the coagulation time has increased with concentration increasing like heparin. However, the coagulation time of heparin was distinctly higher than that of HBPE-SO_3 NPs at the same concentration. The reason may be concluded as follows. For HBPE-SO_3 NPs we prepared, the incomplete sulfonated-terminal modifying with retaining part of hydroxyl groups resulted in the limited number of sulfonate groups, which were proved to be beneficial for anticoagulant effect (Subhapradha et al., 2013).

As shown in Fig. 1D, the binding function between TBA and HBPE-SO_3 NPs was confirmed by UV–vis spectroscopy. Encouragingly, an obvious absorption peak appeared at 255 nm in the mixing solution of TBA and HBPE-SO_3 NPs, in contrast, from 200 to 700 nm, no absorption peak was observed in HBPE-SO_3 NPs. In short, TBA was attached to the HBPE-SO_3 NPs successfully without destroying of the DNA strand (Liu et al., 2013), which was attributed to the good biocompatibility of HBPE-SO_3 NPs.

3.2.2. Whole blood and platelet adhesion assay of HBPE-SO_3 NPs modified electrodes

It is well known that when the foreign materials contact with blood directly, platelets, proteins and other blood components are prone to initiate the formation of clots, and then trigger the coagulation

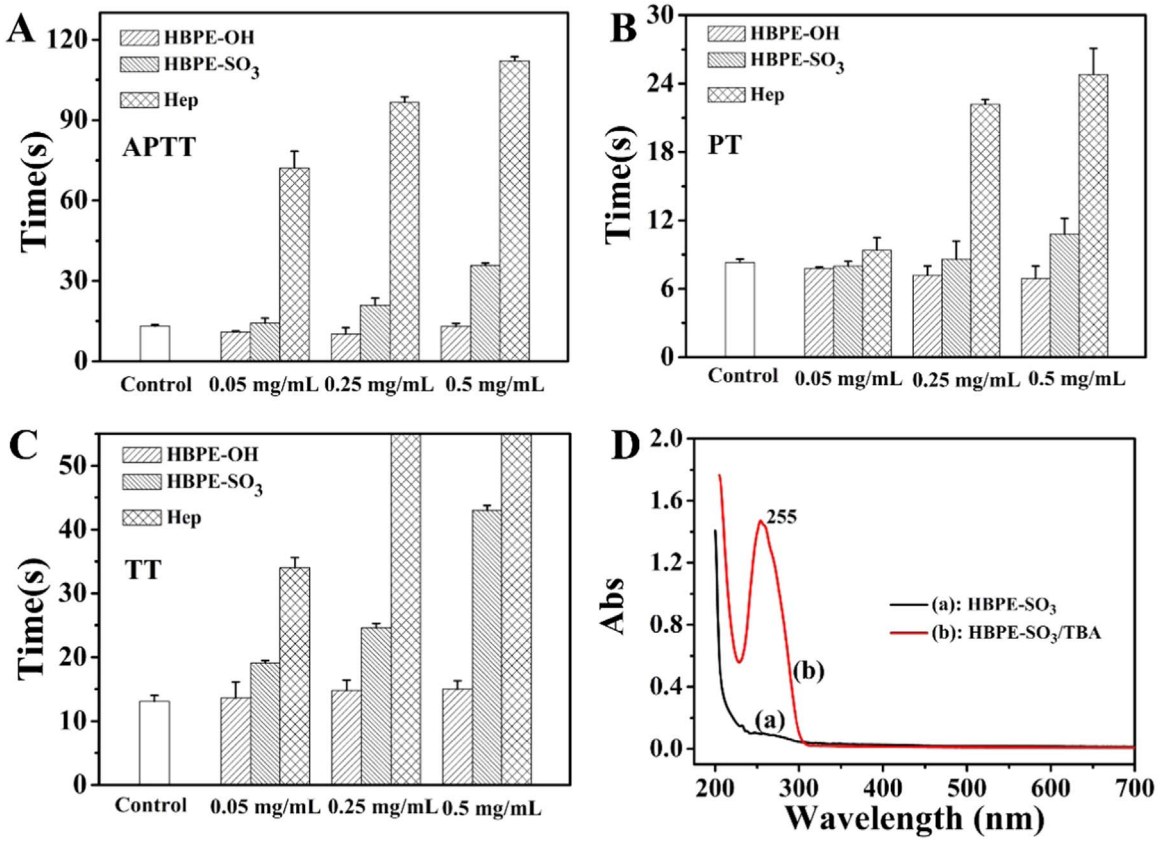

Fig. 1. Coagulation time assay of different concentration of HBPE-SO_3 and heparin including (A) APTT, (B) PT and (C) TT, PBS was used as a control; (D) UV–Vis absorption spectra of (a) HBPE-SO_3 NPs and (b) the mixing solution of HBPE-SO_3 and TBA.

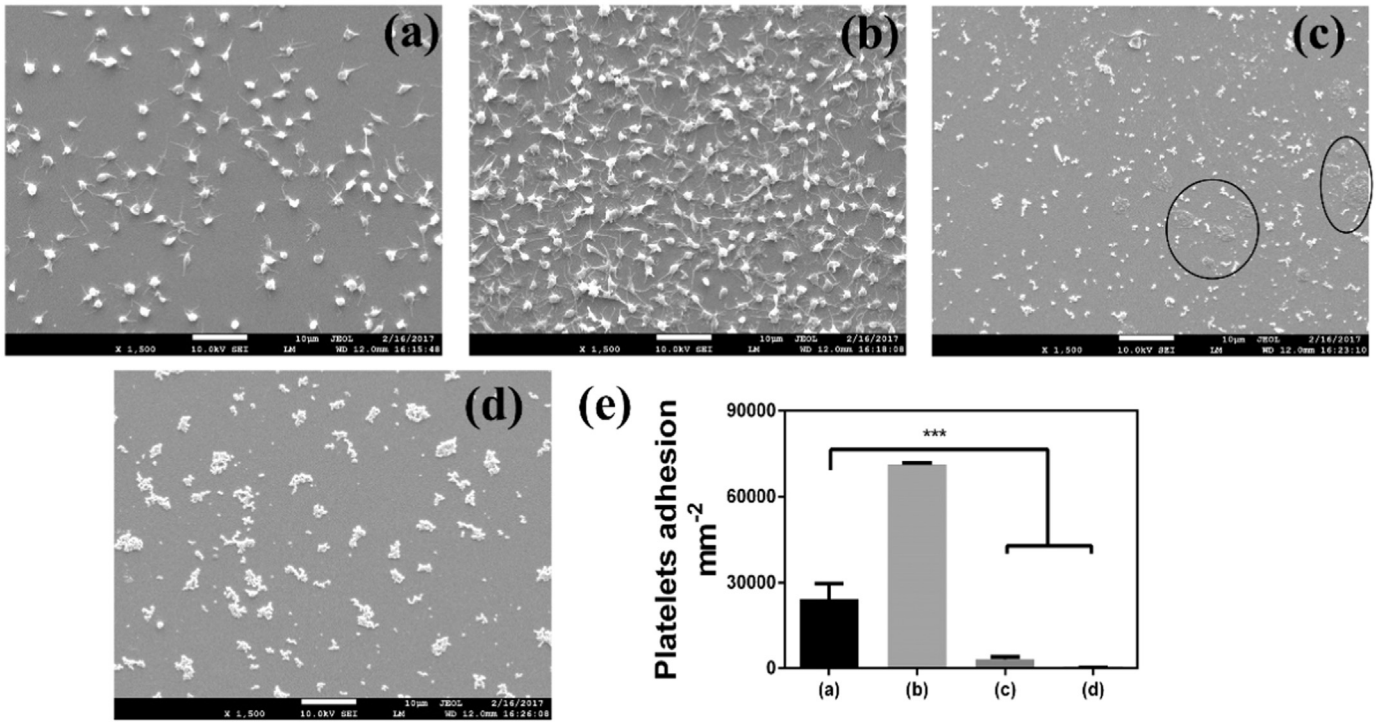

Fig. 2. The adherent platelets morphology of (a) ITO, (b) MPTMS/ITO, (c) Au/MPTMS/ITO and (d) HBPE-SO_3/Au/MPTMS/ITO, scale bar: 10 μm; (e) Quantization of platelet adhesion for different electrodes by statistical analysis. (n = 4, one-way ANOVA with Tukey's post-hoc test, (****, $p < 0.0001$)).

phenomenon (Gorbet and Sefton, 2004). And the electron transfer that occurred between enzyme and electrode redox center will be unwanted damaged because of the biofouling of electrode surface. Therefore, reducing protein adsorption is the crucial for the improvement in hemocompatibility of electrode surface. The SEM results of adhered platelets and red blood cells on different electrodes surfaces were shown in Fig. 2. Many platelets adhered on the surfaces of pristine ITO (Fig. 2a) and MPTMS/ITO (Fig. 2b) and extended their pseudopodia. In the contrast, on the Au/MPTMS/ITO (Fig. 2c) surface the platelets' adhesion decreased, and the few adhered platelets were rupture without extending pseudopodia. And there were almost no adhered platelets was observed on the surface of HBPE-SO_3/Au/MPTMS/ITO (Fig. 2d) with the significant differences (Fig. 2e) in contrast to ITO. The results indicated that the HBPE-SO_3 NPs modified ITO surface could inhibit adhesion and activation of platelets. Additionally, after contacting with fresh whole blood for 1 h, the surface morphologies of different prepared electrodes were shown in Fig. S4. The blood cells adhesion was consistent with the adhesion of platelets, to be more specific, a large number of adherent blood cells with concave discoid morphology were observed on ITO and MPTMS/ITO, whereas no blood cells were observed on the Au/MPTMS/ITO and HBPE-SO_3/Au/MPTMS/ITO surface. The result of statistical analysis illustrated that there was significant difference in anti-biofouling between ITO and HBPE-SO_3/Au/MPTMS/ITO.

3.2.3. Hemolysis assay

Hemolysis method is an important tool to evaluate the biocompatibility of blood-contacting materials, and less than 5% hemolysis is regarded as a nontoxic effect level (Ji et al., 2013; Jiang et al., 2011). Fig. S showed the hemolysis test results of the prepared different samples, which was calculated by the Equ. (S1). In this case, all samples had negligible effects on hemolysis (< 5%). After HBPE-SO_3 NPs modifying electrode, its hemolysis even decreased to 1.46%. The results could be concluded that there was no hemolysis phenomenon when the HBPE-SO_3 NPs modified electrodes contact with the blood.

3.2.4. Morphological changes of RBCs

Generally, when RBCs exposing to the poor blood compatibility materials, the morphology will change into aberrant forms such as echinocyte-like forms with plentiful surface spikes, swollen RBCs, *etc*. Accordingly, the morphology of RBCs is employed to provide further validation for the bioincompatibility of various medical devices except the hemolysis test (Asharani et al., 2010). The images of RBCs after incubating with different electrodes were showed in Fig. S5B. Most of the RBCs still remained the normal morphology with biconcave discoid, especially the morphology of RBCs that incubated with HBPE-SO_3/Au/MPTMS/ITO was almost same as to the negative control group.

All the results indicated that the heparin-mimicking HBPE-SO_3 NPs, showed distinct anticoagulant properties and good hemocompatibility. Furthermore, the ideal anti-biofouling performance was observed on the surface of HBPE-SO_3 NPs modified electrodes, which was essential for the detection of TB in whole blood.

3.3. Characterizations of the fabricated process of aptasensor

Cyclic voltammetry (CV) and electrochemical impedance spectroscopy (EIS) were utilized to monitor the fabrication process of the label-free aptasensor. As shown in Fig. 3, compared with the GCE (curve a), peak current of MPTMS/GCE (curve b) was decreased clearly owing to the poor conductivity of MPTMS molecules. Thus, it was observed that MPTMS/GCE modified by Au NPs possessed the higher peak current (curve c) that compared to MPTMS/GCE. After Au/MPTMS/GCE being modified by HBPE-SO_3 NPs (curve d), TBA (curve e) and TB (curve f) sequentially *via* layer-by-layer assembly method, the amperometric response was corresponding further decreased. In particular, after TBA/HBPE-SO_3/Au/MPTMS/GCE incubating with TB, the amperometric response was decreased obviously. The reasons could be concluded that the electron transfer resistance increased due to the stereo-hindrance effect of G-quadruplex-TB composites generated by TBA and TB. Inset in Fig. 3 was showed the impact on amperometric response resulted from Au and HBPE-SO_3 NPs, peak currents were also observed at the TB/TBA/HBPE-SO_3/MPTMS/GCE (curve g) and TB/TBA/Au/MPTMS/

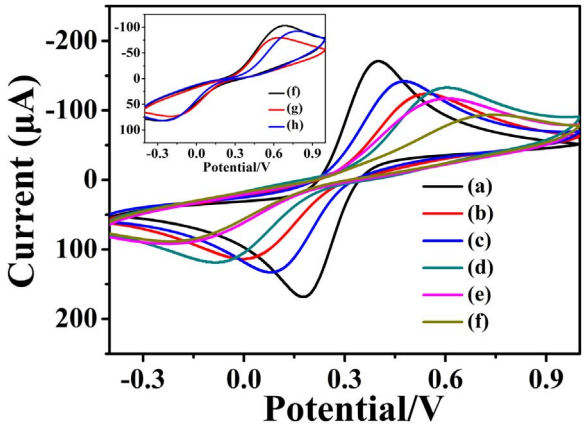

Fig. 3. CV curves of different modified electrodes in 0.1 M PBS (pH 7.4) containing 0.1 M KCl and 10 mM $Fe(CN)_6^{3-/4-}$, (a) GCE, (b) MPTMS/GCE, (c) Au/MPTMS/GCE, (d) HBPE-SO_3/Au/MPTMS/GCE, (e) TBA/HBPE-SO_3/Au/MPTMS/GCE, (f) TB/TBA/HBPE-SO_3/Au/MPTMS/GCE, (g) TB/TBA/HBPE-SO_3/MPTMS/GCE and (h) TB/TBA/Au/MPTMS/GCE, scan rate: 0.1 V/s.

GCE (curve h). But both the peak currents of curve g and curve h were lower than that of curve f, which was because the HBPE-SO_3 with nanoscale effect (Shah et al., 2014) and Au NPs with good conductivity increased the specific surface area for improving loading capacity of TBA and enhanced electron transfer taking place at electrode surface, respectively.

The interface properties of surface-modified electrodes were further characterized by EIS. The typical impedance spectrum is presented in the form of the Nyquist plot, which is composited of the semicircle portion and linear portion corresponding to the higher and lower frequencies, respectively. The semicircle diameter can be quantified as the charge-transfer resistance (Rct), which controls the electron-transfer kinetics of the redox probe at the electrode interface (Kilic et al., 2015; Chiriacò et al., 2015). Therefore, Rct can be used to describe the interface properties of the electrode, whose value varies with different substances modified onto the electrode surface. Fig. S6 showed the impedance spectra observed upon the layer-by-layer self-assembly modification process. The changing of peaks currents in CVs was revealed the electron-transfer, therefore, with which varies in Rct of EIS spectra were in agreement. In short, CVs and EIS indicated the aptasensor was constructed successfully by layer-by-layer self-assembly modification.

3.4. Optimization of conditions

Before evaluating the electrochemical performance of proposed aptasensor, conditions including temperature, incubation time and pH were optimized in Fig. S7. Considering the practical application of proposed aptasensor and the normal physiological temperature, the ambient temperature was used in the further study. Since the formation of G-quadruplex-TB needed time, thus, incubation time between TBA/HBPE-SO_3/Au/MPTMS/GCE and TB was also investigated. It could be seen in Fig. S, the current decreased with the increasing incubation time from 5 min to 20 min, and then the current signals achieved a platform at 40 min implying the specific binding between the TBA and TB was saturated. In addition, taking account of the affect resulted from storage time of the whole blood sample, 20 min was employed to the final

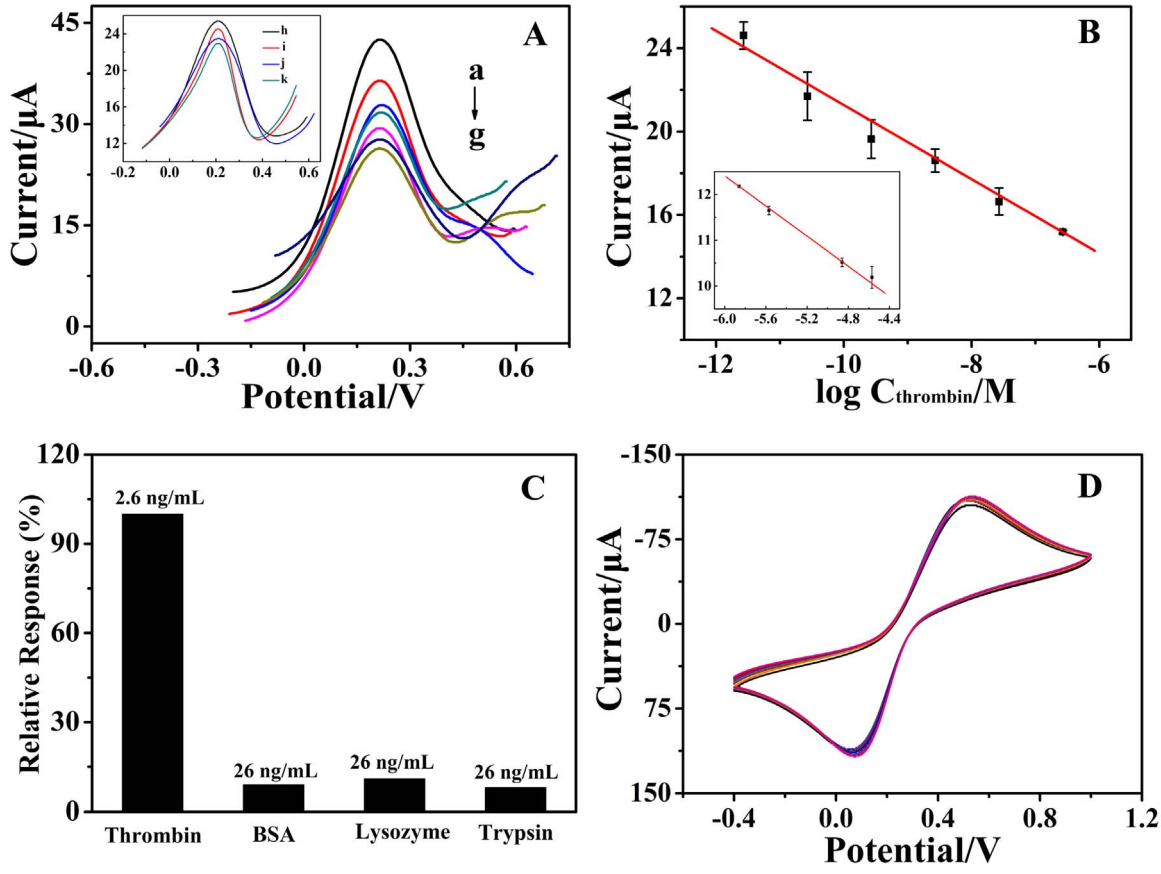

Fig. 4. (A) The DPV plots of different TB concentration obtained at proposed aptasensor (a, b to k corresponding to the concentration from 0 pM, 2.70 pM, 27.0 pM, 0.27 nM, 2.70 nM, 27.0 nM, 0.27 μM, 1.35 μM, 2.70 μM, 13.5 μM and 27.0 μM) in whole blood; (B) Calibration plots upon the addition of varying amounts of TB, inset was the calibration plots upon high TB concentration 1.35–27.0 μM); (C) The specificity of the aptasensor was investigated by DPV in the presence of various interfering antigens and (D) CVs of TBA/HBPE-SO_3/Au/MPTMS/GCE at 30 cycles in 0.1 M PBS (pH 7.4) containing 0.1 M KCl and 10 mM $Fe(CN)_6^{3-/4-}$, scan rate: 0.1 V/s.

Table 1
Comparison of detection of TB concentration using proposed aptasensor and fluorescence methods.

Samples	Aptasensor Concentration (nM)	Fluorescence	Relative deviation (%)
1	11.45	10.41	9.08
2	30.06	29.98	0.27
3	54.67	51.12	6.49

incubation time. More importantly, the protein activity and microstructure would be affected by the environment, such as strongly acidic or alkaline. Consequently, the effect of pH was further studied, as shown in Fig. S7B. The differential pulse voltammetry (DPV) response of biosensor was lowest under the acidic (pH 6.0) and alkaline (pH 8.5) environment, in contrast, pH 7.5 showed the optimal DPV response. So pH 7.4 was selected for the optimal condition, which was closest the physiological condition.

3.5. Electrochemical performances of the prepared aptasensor

The performance of TB/TBA/HBPE-SO_3/Au/MPTMS/GCE was recorded by a series of DPVs corresponding to various concentrations of TB in whole blood under the optimal experimental conditions. As shown in Fig. 4A, the amperometric response decreased with the increase of TB concentration, which could be attributed to the presence of G-quadruplex-TB that can inhibit electron transfer, thereby causing the increase of resistance. And the corresponding calibration curves for thrombin were depicted in Fig. 4B. A linear relationship between the amperometric response and logarithmic value of TB concentration was obtained in a wide concentration range from 2.70 pM to 270 nM and 1.35 μM to 27.0 μM corresponding to the linear equations I (μA) = 3.49-1.78 logC (M) (R^2 = 0.9929) and I (μA) = 2.54-1.64 logC (M) (R^2 = 0.9983), respectively. Generally, the normal concentration of TB in blood during coagulation process was nanomolar level, therefore, TB concentration that could be detected in picomolar range in blood was significant for clinical diagnosis of the related diseases (Yang et al., 2016). Encouragingly, the detection limit was estimated to be 0.031 pM at the signal-to-noise ratio of 3, indicating that the biosensor exhibited excellent performance with fantastically low detection limit compared with the previous biosensor for TB detection by different methods, for example, electrochemiluminescence, chemiluminescence, fluorescence polarization (Table S1). The low detection limit and wide linear range of proposed aptasensor was attributed to the high specific area of HBPE-SO_3/Au/MPTMS/GCE caused by nanoscale effect of HBPE-SO_3 NPs, increasing the loading capacity of TBA.

3.6. Selectivity, stability and reproducibility

The aptasensor with excellent performance should possess high sensitivity for detection of trace target substances, outstanding selectivity for preventing unwanted interference, and excellent stability and reproducibility for long-term storage and recycling. In order to test the selectivity, the signal response was assessed in various interfering antigens containing BSA, lysozyme and trypsin, which coexisted with TB in blood (Li et al., 2012). As shown in Fig. 4C, compared with the current response caused by TB, the relative responses of BSA, lysozyme and trypsin were 9.1%, 11.0% and 8.9%, correspondingly. The phenomenon indicated that the proposed aptasensor had good selectivity in TB detection, which could be explainable as the specific recognition between TBA and TB.

CVs from −0.4 to 0.9 V were employed to further investigate the electrochemical stability of TBA/HBPE-SO_3/Au/MPTMS/GCE over a long time (30 cycles), as shown in Fig. 4D. The result exhibited strong and stable intensity and almost every CV curve overlapped, revealing the excellent chemical and structural stability. Good stability could be attributed to the strong interaction for the layer-by-layer self-assembly modification *via* covalent bond and electrostatic interaction.

The reproducibility of aptasensor was also investigated from the DPV response as shown in Fig. S8. Five fresh electrodes fabricated independently were used to detect 2.69 nM TB, and a relative standard deviation (RSD) of 3.68% was obtained, indicating the prepared aptasensor had satisfactory electrode-to-electrode reproducibility.

3.7. Analysis of real samples

Based on the results of anti-biofouling properties of proposed aptasensor, in order to demonstrate the analytical reliability and practical applicability, the aptasensor prepared independently was used to determine the concentration of TB in whole blood directly that supplied by donors from the local hospital. Table 1 showed the comparison between the values obtained by the proposed aptasensor in whole blood and the reference values obtained by the fluorescence method (Jin et al., 2010) in serum samples. The results indicated there was no significant difference between the two values with low relative deviation, and values measured in whole blood were a slight higher than that in serum samples. Furthermore, taking account of the wastage of TB caused by necessary centrifugation for getting serum samples, therefore, the results that measured in whole blood by the aptasensor we proposed was more reliable due to the being closer to the actual values. Thus, the aptasensor can be used for determination of TB in whole blood sample directly.

4. Conclusions

In this case, heparin-mimicking HBPE-SO_3 NPs were synthesized successfully and proved to have significant antithrombogenicity that attributed to their abundant of sulfonated functional end-groups. And then a novel label-free and sensitive aptasensor based on HBPE-SO_3 NPs modified electrode was prepared and applied in whole blood for TB detection directly by help of the anti-biofouling properties of electrodes interface, which had distinct advantages in accuracy compared with the other reported aptasensor that applied in human serum. What's more, nano-sized effect and high density of terminal groups of HBPs played key role in constructing novel biosensor platform with high electrochemical performances. Accordingly, the collaborative innovation strategy that involved hyperbranched architecture, nano-sized effect, layer-by-layer self-assembly and biosensor technology we proposed will provide more possibilities to high-performance biosensors that are relevant to early diagnostics and therapy of human diseases.

Acknowledgements

The work was supported by National Natural Science Foundation of China (51641104, 21603105, 21571104), Jiangsu Agricultural Science and Technology Innovation Fund Project (CX(14)2127), Technology Support Program of Science and Technology Department of Jiangsu Province (BE2015703), Jiangsu Key Technology RD Program (BE2016010), the Priority Academic Program Development of Jiangsu Higher Education Institution, Major Projects of Natural Sciences of University in Jiangsu Province of China (14KJA150006), Chinese Postdoctoral Science Foundation (2015M580446), and Huaian Key Research and Development Program (HAG201621).

Appendix A. Supplementary material

Supplementary data associated with this article can be found in the online version at http://dx.doi.org/10.1016/j.bios.2017.10.037.

References

Aaldering, L.J., Poongavanam, V., Langkjær, N., Murugan, N.A., Jørgensen, P.T., Wengel, J., Veedu, R.N., 2017. ChemBioChem 18, 755–763.
Arab Chamjangali, M., Kouhestani, H., Masdarolomoor, F., Daneshinejad, H., 2015. Sens. Actuators B-Chem. 216, 384–393.
Asharani, P.V., Sethu, S., Vadukumpully, S., Zhong, S.P., Lim, C.T., Hande, M.P., Valiyaveettil, S., 2010. Adv. Funct. Mater. 20, 1233–1242.
Capila, I., Linhardt, R.J., 2002. Angew. Chem. Int. Ed. 41, 390–412.
Chiriacò, M.S., Feo, F.D., Primiceri, E., Monteduro, A.G., Benedetto, G.E.D., Pennetta, A., Rinaldi, R., Maruccio, G., 2015. Talanta 142, 57–63.
Cui, M., Song, Z., Wu, Y., Guo, B., Fan, X., Luo, X., 2016. Biosens. Bioelectron. 79, 736–741.
Cuker, A., Siegal, D.M., Crowther, M.A., Garcia, D.A., 2014. J. Am. Coll. Cardiol. 64, 1128–1139.
Ding, D., Wang, G., Liu, J., Li, K., Pu, K.Y., Hu, Y., Ng, J.C.Y., Tang, B.Z., Liu, B., 2012. Small 8, 3523–3530.
Gao, F.L., Du, L.L., Tang, D.Q., Lu, Y., Zhang, Y.Z., Zhang, L.X., 2015. Biosens. Bioelectron. 66, 423–430.
Gorbet, M.B., Sefton, M.V., 2004. Biomaterials 25, 5681–5703.
Han, Q., Chen, X., Niu, Y., Zhao, B., Wang, B., Mao, C., Chen, L., Shen, J., 2013. Langmuir 29, 8402–8409.
Hao, C., Yan, F., Ding, L., Xue, Y., Ju, H., 2007. Electrochem. Commun. 9, 1359–1364.
He, M., Cui, X., Jiang, H., Huang, X., Zhao, W., Zhao, C., 2017. Macromol. Biosci. 17, 1600281.
Heydari-Bafrooei, E., Amini, M., Ardakani, M.H., 2016. Biosens. Bioelectron. 85, 828–836.
Huang, X., Wang, R., Lu, T., Zhou, D., Zhao, W., Sun, S., Zhao, C., 2016. Biomacromolecules 17, 4011–4020.
Huang, Y., Shaw, M.A., Mullins, E.S., Kirley, T.L., Ayres, N., 2014. Biomacromolecules 15, 4455–4466.
Ji, X., Yang, W., Wang, T., Mao, C., Guo, L., Xiao, J., He, N., 2013. J. Biomed. Nanotechnol. 9, 1672–1678.
Jiang, H., Wang, X.B., Li, C.Y., Li, J.S., Xu, F.J., Mao, C., Yang, W.T., Shen, J., 2011. Langmuir 27, 11575–11581.
Jin, Y., Bai, J., Li, H., 2010. Analyst 135, 1731–1735.
Kilic, T., Erdem, A., Erac, Y., Seydibeyoglu, M.O., Okur, S., Ozsoz, M., 2015. Electroanalsis 27, 317–326.
Li, Y., Liu, L., Fang, X., Bao, J., Han, M., Dai, Z., 2012. Electrochim. Acta 65, 1–6.
Liu, H., Xu, S., He, Z., Deng, A., Zhu, J.J., 2013. Anal. Chem. 85, 3385–3392.
Paluck, S.J., Nguyen, T.H., Maynard, H.D., 2016. Biomacromolecules 17, 3417–3440.
Shah, M.A., He, N., Li, Z., Ali, Z., Zhang, L., 2014. J. Biomed. Nanotechnol. 10, 2332–2349.
Shen, G., Zhang, H., Yang, C., Yang, Q., Tang, Y., 2017. Anal. Chem. 89, 548–551.
Subhapradha, N., Ramasamy, P., Srinivasan, A., Madeswaran, P., Shanmugam, V., Shanmugam, A., 2013. Int. J. Biol. Macromol. 62, 336–340.
Sun, A.L., Qi, Q.G., Wang, X.N., Bie, P., 2014. Biosens. Bioelectron. 57, 16–21.
Tamada, Y., Murata, M., Hayashi, T., Goto, K., 2002. Biomaterials 23, 1375–1382.
Wen, J., Weinhart, M., Lai, B., Kizhakkedathu, J., Brooks, D.E., 2016. Biomaterials 86, 42–55.
Wu, W., Tang, R., Li, Q., Li, Z., 2015. Chem. Soc. Rev. 44, 3997–4022.
Wang, L., Su, B., Cheng, C., Ma, L., Li, S., Nie, S., Zhao, C., 2015. J. Mater. Chem. B 3, 1391–1404.
Wang, T., Ji, X., Jin, L., Feng, Z., Wu, J., Zheng, J., Wang, H., Xu, Z.W., Guo, L., He, N., 2013a. ACS Appl. Mater. Interfaces 5, 3757–3763.
Wang, X., Chen, X., Xing, L., Mao, C., Yu, H., Shen, J., 2013b. J. Mater. Chem. B 1, 5036–5044.
Wang, X., Miao, J., Shao, X., Mao, C., Shen, J., 2014. J. Colloid Interface Sci. 420, 88–96.
Xi, Z., Huang, R., Li, Z., He, N., Wang, T., Su, E., Deng, Y., 2015. ACS Appl. Mater. Interfaces 7, 11215–11223.
Xiao, Y., Lubin, A.A., Heeger, A.J., Plaxco, K.W., 2005. Angew. Chem. Int. Ed. 44, 5456–5459.
Xu, W.J., Xue, S.Y., Yi, H.Y., Jing, P., Chai, Y.Q., Yuan, R., 2015. Chem. Commun. 51, 1472–1474.
Yang, J., Dou, B., Yuan, R., Xiang, Y., 2016. Anal. Chem. 88, 8218–8223.
Yu, B., Jiang, X., Wang, R., Yin, J., 2010. Macromolecules 43, 10457–10465.
Zhang, Z., McCallum, S.A., Xie, J., Nieto, L., Corzana, F., Jiménez-Barbero, J., Chen, M., Liu, J., Linhardt, R.J., 2008. J. Am. Chem. Soc. 130, 12998–13007.
Zheng, Y., Li, S., Weng, Z., Gao, C., 2015. Chem. Soc. Rev. 44, 4091–4130.